A complement factor H homolog, heparan sulfation, and syndecan maintain inversin compartment boundaries in *C. elegans* cilia

Natalie Acker[a], Harold Smith[b], Claire Devine[a], Sharon L. Oltjen[c], Sofia Tsiropoulou[d], Zeljka Smit-McBride[c], Karen Lange[d], Oliver E. Blacque[d], Joanne A. Matsubara[e], Andrew Gordus[f], Andy Golden[b], and Bruce E. Vogel[a,g,1]

[a]Center for Biomedical Engineering and Technology, University of Maryland School of Medicine, University of Maryland, Baltimore, MD 21201; [b]Laboratory of Biochemistry and Genetics, National Institute of Diabetes, Digestive, and Kidney Diseases, NIH, Bethesda, MD 20892; [c]Department of Ophthalmology and Vision Science, Vitreoretinal Research Laboratory, University of California, Davis, CA 95616; [d]School of Biomolecular and Biomedical Research, UCD Conway Institute, University College Dublin, Belfield, Dublin 4, Ireland; [e]Department of Ophthalmology and Visual Sciences, The University of British Columbia, Vancouver, BC V5Z 3N9, Canada; [f]Department of Biology, The Johns Hopkins University, Baltimore, MD 21211; and [g]Department of Physiology, University of Maryland School of Medicine, University of Maryland, Baltimore, MD 21201

Edited by Iva Greenwald, Columbia University, New York, NY, and approved March 4, 2021 (received for review August 6, 2020)

Age-related macular degeneration (AMD) is a leading cause of blindness among the elderly. Canonical disease models suggest that defective interactions between complement factor H (CFH) and cell surface heparan sulfate (HS) result in increased alternative complement pathway activity, cytolytic damage, and tissue inflammation in the retina. Although these factors are thought to contribute to increased disease risk, multiple studies indicate that noncanonical mechanisms that result from defective CFH and HS interaction may contribute to the progression of AMD as well. A total of 60 ciliated sensory neurons in the nematode *Caenorhabditis elegans* detect chemical, olfactory, mechanical, and thermal cues in the environment. Here, we find that a *C. elegans* CFH homolog localizes on CEP mechanosensory neuron cilia where it has noncanonical roles in maintaining inversin/NPHP-2 within its namesake proximal compartment and preventing inversin/NPHP-2 accumulation in distal cilia compartments in aging adults. CFH localization and maintenance of inversin/NPHP-2 compartment integrity depend on the HS 3-*O* sulfotransferase HST-3.1 and the transmembrane proteoglycan syndecan/SDN-1. Defective inversin/NPHP-2 localization in mouse and human photoreceptors with CFH mutations indicates that these functions and interactions may be conserved in vertebrate sensory neurons, suggesting that previously unappreciated defects in cilia structure may contribute to the progressive photoreceptor dysfunction associated with CFH loss-of-function mutations in some AMD patients.

complement factor H | heparan sulfate | syndecan | cilia | inversin

Age-related macular degeneration (AMD) is the leading cause of blindness among the elderly in the developed world, affecting 11% of adults over the age of 85. Although the discovery of a Y402H variant in complement factor H (CFH) as a major risk factor for AMD marked a major advance for the field, the roles of CFH and Y402H in the mechanisms of disease initiation and progression remain unclear (1–5).

The alternative pathway is one of three complement system pathways that are part of the innate immune system's natural defense against infections. The canonical function of CFH in modulating alternative complement pathway activity suggests a central role for excessive alternative complement pathway activity in the progressive photoreceptor dysfunction that is characteristic of AMD pathogenesis (1–8). CFH is a secreted protein composed of 20 complement control protein (CCP) repeats (also known as short complement repeats (SCRs) or sushi domains) that inhibits alternative complement pathway-associated inflammation and cytolysis on host cell surfaces by promoting decay of the convertase that cleaves and activates C3 and also by acting as a cofactor for factor I in processing C3b to its inactive form (9).

CFH interacts with host cell surfaces by binding to heparan sulfate (HS) through binding sites found in CCP 7 and CCP 19 to 20 (10). HSs are heterogenous repeats of glucuronic acid and *N*-acetylglucosamine disaccharide covalently attached to proteoglycan core proteins that may be transmembrane such as the syndecans, glycosylphosphatidylinositol-anchored proteins such as the glypicans, or secreted such as perlecan, agrin, and collagen XVIII (11–14).

HS heterogeneity results from variation in disaccharide length and partial deacetylation, epimerization, and modification by 2-, 3-, and 6-*O* sulfotransferases (15). Sequence variants within HS binding sites in CFH, including Y402H in CCP 7, result in reduced HS affinity, suggesting that increased AMD risk is a result of reduced CFH on cell surfaces and increased alternative complement pathway activity within the retina (16).

However, CFH is also reported to have functions outside its canonical role in regulating the alternative complement pathway that include preventing lipid binding to HS and modulating monocyte migration (17, 18). This suggests that noncanonical mechanisms may contribute to the dysfunction and death of photoreceptor cells that are associated with AMD progression.

Significance

Mutations in complement factor H (CFH) binding sites for heparan sulfate (HS) increase risk for age-related macular degeneration (AMD), but the roles of CFH and HS in disease pathogenesis remain unclear. Here, we find that a CFH homolog, HS modification, and the HS proteoglycan syndecan/SDN-1 have roles in maintaining cilia compartment boundaries in the sensory neurons of aging *C. elegans* adults. The role of CFH in cilia compartment boundaries is conserved in vertebrate photoreceptors, suggesting that structural defects in photoreceptor cilia make a contribution to AMD progression in patients with CFH mutations that has not been appreciated previously.

Author contributions: B.E.V. designed research; N.A., H.S., C.D., S.L.O., S.T., A. Gordus, A. Golden, and B.E.V. performed research; Z.S.-M., K.L., and J.A.M. contributed new reagents/analytic tools; O.E.B. analyzed data; and B.E.V. wrote the paper.

The authors declare no competing interest.

This article is a PNAS Direct Submission.

[1]To whom correspondence may be addressed. Email: bvogel@som.umaryland.edu.

This article contains supporting information online at https://www.pnas.org/lookup/suppl/doi:10.1073/pnas.2016698118/-/DCSupplemental.

Published April 15, 2021.

In addition to increased AMD-risk, the CFH Y402H variant is also associated with increased risk for a defect in rod-mediated dark adaptation (RMDA) that is detectable prior to other clinical AMD symptoms. This suggests that a neuronal signaling defect involving CFH may be an early contributor to AMD-associated neuronal dysfunction (19). In support of this concept, many of the clinical symptoms associated with AMD can be reproduced by defects in structural and signaling proteins associated with photoreceptor outer segments, which are modified primary cilia (20, 21).

Primary cilia are highly compartmentalized microtubule-based protrusions with conserved compositions and organizations containing (from proximal to distal) a transition zone, middle, and distal segment [TZ, MS, DS (22)]. Within the MS, a number of cilia subtypes in mammals and invertebrates (including *Caenorhabditis elegans*) possess a domain called the "inversin compartment," defined by a specific localization of the ciliopathy protein, inversin [also called NPHP2 (23–25)]. Defects in inversin/NPHP-2 may cause left-right body asymmetry for which inversin is named and the early onset cystic kidney disease, nephronophthisis-2 [NPHP-2 (23, 26)]. Within the inversin compartment, inversin/NPHP-2 assembles into filaments of variable length depending on cell type, suggesting the presence of an unknown mechanism, not bound by an obvious structure or membrane, that regulates inversin/NPHP-2 filament length (27, 28).

Here, we find that a *C. elegans* structural homolog of CFH localizes on a subset of mechanosensory neuron primary cilia in a syndecan- and heparan 3-*O* sulfotransferase–dependent manner where it prevents inversin/NPHP-2 from accumulating in distal cilia compartments in aging adults. Similar observations that CFH restricts ectopic inversin/NPHP-2 accumulation in vertebrate photoreceptors suggests that previously unappreciated defects in cilia organization may contribute to photoreceptor dysfunction in AMD patients with CFH mutations in HS binding sites.

Results

Identification of CFH-1, a Structural and Functional Homolog of Vertebrate CFH in *C. elegans*. A candidate for a *C. elegans* homolog of vertebrate CFH, F36H2.3 (NP_001335526.1), was identified in an earlier study (29). CFH and full-length F36H2.3 (https://wormbase.org//species/c_elegans/gene/WBGene00009500#0eg%E2%80%9310) are 1,231 and 1,643 amino acid proteins, respectively, with signal sequences followed by 20 tandem CCP modules and no transmembrane domains. Although F36H2.3 is annotated as an ortholog of human CR2 (complement C3d receptor 2) in some databases and human CFH in others (30), functional overlap with CR2 seems unlikely since CR2 has a transmembrane domain that is not found in either CFH or F36H2.3. The clear overlap in structural organization (*SI Appendix*, Figs. S1 and S2), in tandem with functional data shown below, indicates that F36H2.3 is a more likely structural and functional homolog of vertebrate CFH. We therefore refer to the F36H2.3 gene as *cfh-1* (CFH homolog) and refer to its protein product as CFH-1 to distinguish between vertebrate and nematode proteins.

***cfh-1* Expression by Mechanosensory Neurons and Select Epithelia.** To investigate *cfh-1* expression, a transcriptional reporter, *cfh-1p*::green fluorescent protein (GFP), containing ~3.0 kb of 5′ regulatory sequence fused immediately upstream of GFP (31) was expressed in wild-type (WT) animals. Based on distinctive cell shapes and positions, expression was observed in amphid and phasmid sheath glia and uterine-seam transitional epithelia (utse) in addition to neuronal cells that appear to be dopaminergic posterior deirid (PDE) mechanosensory neurons (Fig. 1*A*). Further investigation of *cfh-1p*::GFP expression in tandem with red fluorescent protein expressed under the control of a *dat-1* promoter, revealed that in addition to 2 PDE neurons, *cfh-1p*::GFP is expressed in 2 anterior deirid (ADE) neurons and 4 cephalic (CEP) ciliated dopaminergic neurons found in the *C. elegans* head (Fig. 1*B*). Based on the canonical function of CFH, this protein would be expected to regulate alternative complement pathway activity. Since a role for this protein consistent with its expression by dopaminergic mechanosensory neurons is not obvious, it was investigated further.

CFH-1 Assembles on the MS of Mechanosensory Neuron Cilia. To determine whether the *cfh-1* gene product, CFH-1, remains associated with the dopaminergic neuron sites of synthesis (Fig. 1*B*), or is secreted and accumulates in another location, a GFP tag was inserted in frame between the signal peptide cleavage site and the first CCP module of endogenous *cfh-1* coding sequence using CRISPR-Cas9 technology (*SI Appendix*, Fig. S2*A*) (32). Analysis of CFH-1::GFP localization reveals a restricted association with the eight ciliated dopaminergic mechanosensory neurons described above (4 CEP, 2 ADE, and 2 PDE), in addition to six nearby outer labial (OL) mechanosensory neurons and a limited number of interfacial epithelia (cells that attach internal tissue to epidermal tissue or to openings in the epidermal tissue to the exterior) that include amphid and phasmid sheath glia, utse, and anterior arcade cells (Fig. 1 *C* and *D* and *SI Appendix*, Fig. S2*B*).

CFH-1::GFP is concentrated along the sensory cilium of CEP mechanosensory neurons, decorating a proximal domain located ~3 to 4 μm from the distal tip of the organelle (Fig. 1*D*). CFH-1 is located distal to the TZ protein MKSR-1, indicating that the CFH-1::GFP signal likely corresponds to the ultrastructurally defined MS of this cilium subtype (*SI Appendix*, Fig. S2*C*) (33). Within the MS, a number of ciliary subtypes in mammals and invertebrates (including *C. elegans*) possess a proximal ciliary domain called the "inversin compartment," defined by a specific localization of the protein, inversin/NPHP-2 (23–25). CFH-1::GFP localization was examined in tandem with inversin compartment marker NPHP-2::mCherry expressed under control of the dopaminergic neuron-specific *dat-1* promoter (24, 34–36). In agreement with previous findings, we find that NPHP-2::mCherry localizes in a proximal region of the CEP cilium in WT animals (Fig. 1*E*) (24, 25, 34–36). CFH-1::GFP localization is concentrated at a region of the MS with partial overlap of NPHP-2::mCherry (i.e., the inversin compartment) and extends distally through the junction between the MS and DS (Fig. 1*E*).

CFH-1 Prevents Inversin/NPHP-2 from Accumulating in the Distal Cilia Compartment in *C. elegans* Mechanosensory Neurons. Based on its position near the junction between MS and DS, we next determined whether CFH-1 has an influence on the distributions of inversin/NPHP-2, MS component ARL-13, and DS component TRP-4 (37, 38). WT animals were compared with two independently isolated *cfh-1* null alleles: one with a frameshift deletion of seven nucleotides from the *cfh-1* coding sequence prior to the first CCP module created using CRISPR-Cas9 technology [*cfh-1(em14)*] and a second deletion mutant [*cfh-1(gk3206)*] that is missing 300 bp of exon 1 sequence encoding the initiator methionine and signal peptide (F36H2 25,831-26,130) (39).

Inversin/NPHP-2 has a restricted distribution within the MS in day 1, 2, and 3 WT adults, and there is no significant differences between WT and two independent *cfh-1* mutant day 1 adults. However, in day 2 and 3, *cfh-1* mutant adults, inversin/NPHP-2::mCherry extends ectopically into the DS of CEP neuron cilia (Fig. 2*A*). This mutant phenotype is rescued by a genomic fragment containing endogenous CFH-1 regulatory and coding sequence and a construct with *cfh-1* expression under the control of the dopaminergic neuron-specific *cat-2* promoter. This data not only demonstrates that inversin/NPHP-2::mCherry mislocalization observed in aging *cfh-1* mutant animals is due to *cfh-1* loss of function but also shows that *cfh-1* can function in a cell-autonomous manner (Fig. 2 *A* and *C*). In contrast to the defect in inversin/NPHP-2::mCherry distribution, there was little

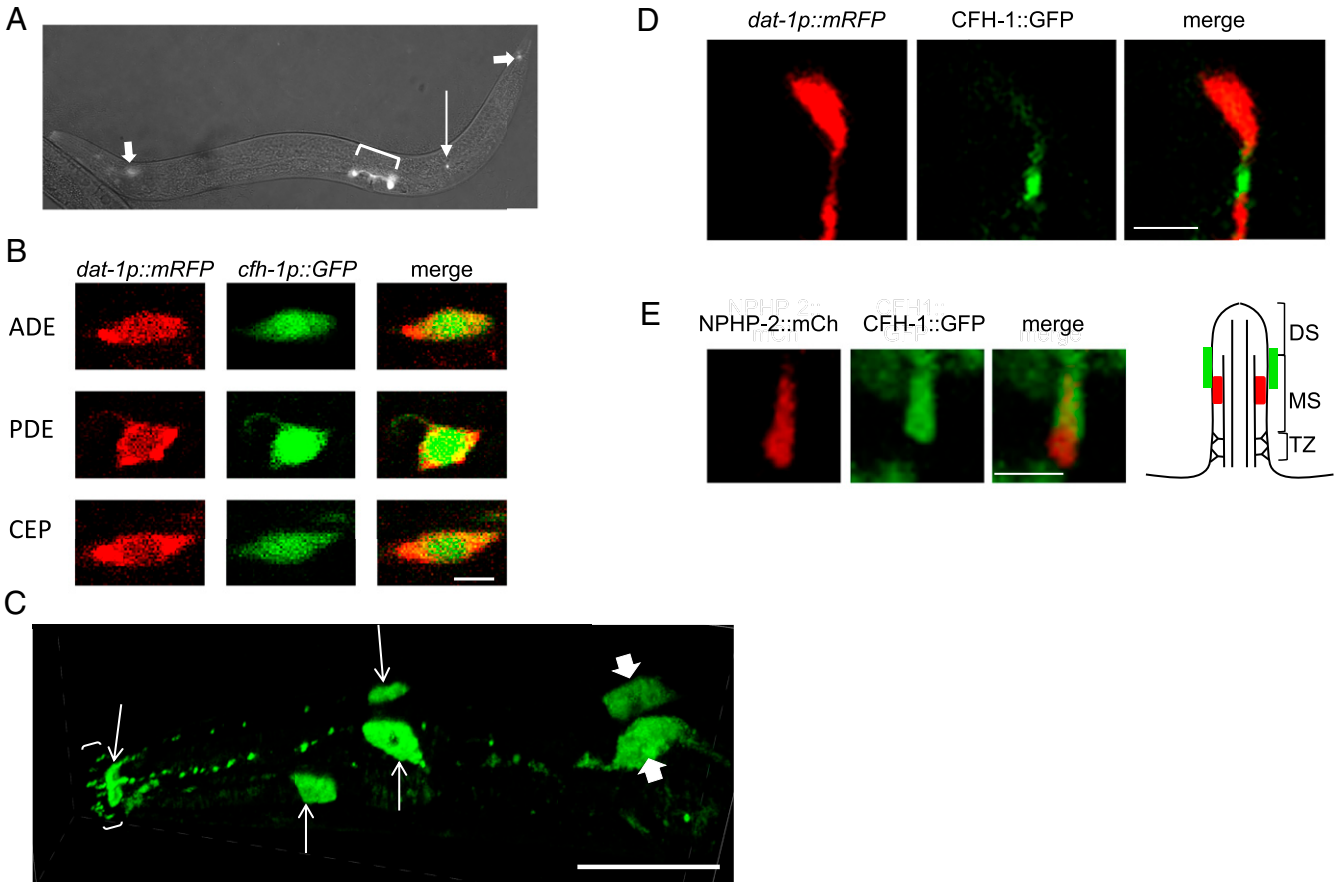

Fig. 1. *cfh-1* expression and CFH-1::GFP localization on CEP mechanosensory neuron cilia. (*A*) GFP expressed under the control of *cfh-1* 5′ untranslated regulatory sequence in young adult animal. GFP fluorescence is detected in amphid and phasmid sheath glial cells (thick arrows), H-shaped uterine-seam epithelial cell (bracket), and PDE dopaminergic mechanosensory neurons (thin arrow). Anterior is oriented left. (*B*) *cfh-1* promoter driving GFP expression and *dat-1* promoter driving monomeric red fluorescent protein (mRFP) expression overlap in dopaminergic ADE, PDE, and CEP mechanosensory neuron cell bodies (Scale bar, 2.5 μm). (*C*) CFH-1::GFP localization on sensory neurons and interfacial epithelia in L4 animals. CFH-1::GFP translational fusion protein is detected on four CEP neurons and four outer labial quadrant and two outer labial lateral mechanosensory neurons (brackets). CFH-1::GFP is also located on the anterior arcade cell syncytium (left arrow) and cell bodies (thin right arrows) and is also found on amphid sheath cells (thick right arrows). Anterior is oriented left (Scale bar, 25 μm). (*D*) Confocal image of CFH-1::GFP translational fusion in tandem with mRFP under the control of dopaminergic neuron–specific *dat-1* promoter in CEP sensory neurons. (Scale bar, 2.5 μm). Anterior is oriented up. (*E*) Confocal image of inversin/NPHP-2::mCherry in tandem with CFH-1::GFP in CEP sensory neuron. Note the partial overlap in localization between inversin/NPHP-2 and CFH-1 (Scale bar, 1 μm). (*Right*) A schematic diagram of cilia showing approximate location of CFH-1 (green) and inversin/NPHP-2 (red) with respect to MS. Also shown are DS and TZ. Anterior is oriented up.

or no detectable difference in ARL-13::mNG and TRP-4::GFP distribution between WT and *cfh-1* mutant animals, regardless of age (Fig. 2). This suggests that the absence of CFH-1 has a specific effect on inversin/NPHP-2 and does not cause a general defect in cilia structure and organization.

In addition to the defect in CEP neuron inversin/NPHP-2 compartment length described above, inversin/NPHP-2 compartment length was measured in inner labial (IL) and OL neurons in day 3 adults. A slight but significant difference in inversin/NPHP-2 compartment size was detected in IL neurons, but no difference was detected in OL neurons (*SI Appendix*, Fig. S3). This provides supporting evidence that the role of CFH-1 in inversin/NPHP-2 compartment maintenance is limited to specific cellular contexts and is not a general role common to all cilia.

***cfh-1* Mutant Animals Have a Defect in Mechanosensory Neuron Function.** Mechanosensory CEP neurons are activated and release dopamine when moving animals encounter food, causing the animals to slow down and forage. To determine whether absence of CFH-1 and the ectopic accumulation of inversin/NPHP-2 in distal cilia compartments results in a defect in CEP neuron activation, a genetically encoded calcium indicator, GCaMP6s, was used to monitor calcium-induced fluorescence in the CEP neurons of WT and *cfh-1(em14)* mutant animals. There was little or no detectable difference in GCAMP6s fluorescence between WT and *cfh-1(em14)* mutant day 1 adults. However, WT day 3 adults have an obvious increase in GCAMP6s fluorescence in CEP neurons upon crossing the threshold of a bacterial lawn due to an influx of calcium that is not observed in day 3 *cfh-1(em14)* mutant animals (*SI Appendix*, Fig. S4*A*).

A defect in CEP neuron activation, as indicated by lack of calcium response, is likely to result in a corresponding behavioral defect, detectable by a previously described "basal slowing" assay that measures the slowing response of *C. elegans* upon encountering food (40, 41). A "blinded" experimenter, unaware of the genotype of the strains being tested, found that WT animals slow dramatically upon encountering a lawn of *Escherichia coli* HB101 while dopamine-synthesis–defective *cat-2(e1112)* mutants have defects in "basal slowing" that are consistent with previous findings (40, 41). In day 1 of adulthood, *cfh-1(em14)* mutant adults demonstrate little or no difference in slowing response when compared to WT animals of the same age. However, by day 3 of adulthood, *cfh-1(em14)* mutant animals have a statistically significant defect in slowing response upon encountering food when

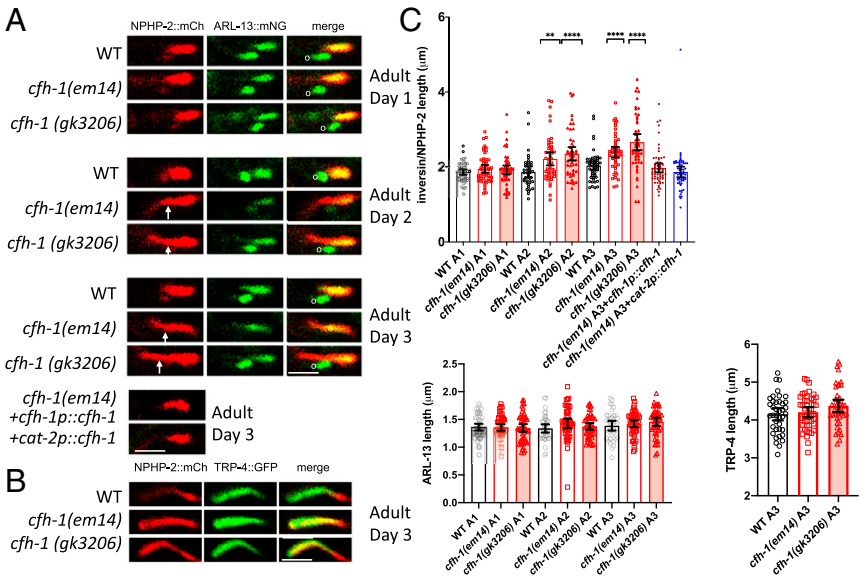

Fig. 2. CFH-1 prevents ectopic accumulation of inversinNPHP-2 in distal cilia compartments. (*A*) Comparison of inversin/NPHP-2::mCherry and ARL-13::mNG localization in CEP neurons of WT, *cfh-1(em14)*, and *cfh-1(gk3206)* mutant animals. Adult day 1, 2, and 3 animals arranged from top to bottom, followed by *cfh-1(em14)* adult day 3 animals containing *cfh-1p::cfh-1* and *cat-2p::cfh-1* transgenes. Note that inversin/NPHP-2 is restricted in length in WT animals but extends into ciliary distal segment in day 2 and 3 mutant adults (arrows) (Scale bar, 2 μM). Anterior is oriented left in all images (nota bene in many of the images, an OL neuron that also expresses ARL-13::mNG is visible adjacent to CEP and is indicated by a lowercase "o"). (*B*) Comparison of inversin/NPHP-2::mCherry and TRP-4::GFP localization in WT (*Top*), *cfh-1(em14)*, and *cfh-1(gk3206)* mutant animals (Scale bar, 5 μm). Anterior is oriented left in all images. (*C*, *Top*) Scatter plots of inversin/NPHP-2 length in adult day 1, 2, and 3 animals and *cfh-1(em14)* adult day 3 animals containing *cfh-1p::cfh-1* and *cat-2p::cfh-1* transgenes. Also shown are ARL-13 lengths in day 1, 2, and 3 adults and TRP-4 lengths in day 3 adults. The error bars indicate 95% CIs. Inversin/NPHP-2 lengths in day 2 and 3 *cfh-1* mutant animals have statistically significant differences from WT. The significance is indicated by brackets with asterisks as follows: $^{**}P < 0.01$ and $^{****}P < 0.0001$. Measurements shown without brackets above are not statistically different from WT.

compared to WT adults of the same age (*SI Appendix*, Fig. S4*A*). Importantly, animals expressing CFH-1::GFP are not statistically different from WT animals, indicating that the CFH-1::GFP fusion protein described above is functional and that localization of the in-frame insertion of GFP into the endogenous *cfh-1* gene product is likely to be representative of WT CFH-1 localization.

We also asked whether the absence of CFH-1 might cause an obvious early disruption of cilia ultrastructure that might cause the observed defects in inversin/NPHP-2 protein localization. However, ultrastructural analysis of CEP neurons found no defects in the TZ, MS, and DS compartments of day 1 adult *cfh-1* mutants (*SI Appendix*, Fig. S4*B*). It is conceivable that ultrastructural defects might arise later in adulthood, but that was not examined.

Inversin/NPHP-2 and CFH-1 Localization Are Dependent on HS Modification. The presence of a signal sequence and 80 conserved disulfide-bond–forming cysteines in 20 tandem CCP modules (*SI Appendix*, Figs. S1 and S2) indicates that CFH-1, like vertebrate CFH, has the hallmarks of a secreted protein. Since inversin/NPHP-2 is a cytoplasmic protein that assembles into fibrils located between the ciliary membrane and axoneme (28), a mechanism for the CFH-1–dependent localization of inversin/NPHP-2 shown above (Fig. 2) is not obvious. To identify components of the mechanism responsible for CFH-1–dependent localization of inversin/NPHP-2, a genome-wide screen designed to identify loss-of-function mutations in genes essential for both inversin/NPHP-2 and CFH-1 localization was performed following random mutagenesis of the *C. elegans* genome (*Materials and Methods*). A mutant *(em15)* with simultaneous disruption of both NPHP-2::mCherry and CFH-1::GFP localization in CEP neurons (Fig. 3*B*) was mapped using molecular inversion probes (MIP) (42) and localized to a small region of LGII. Sequence analysis of this region identified *hst-3.1* as a good candidate gene since it encodes an enzyme important for 3-*O* sulfation of HS (known to bind directly to vertebrate CFH), and the missense mutation identified replaces a proline in HST-3.1 that is highly conserved in vertebrate HS 3-*O* sulfotransferases (Fig. 3*A*; 43). Support for the importance of HS and its 3-*O* sulfotransferase in CFH-1 and inversin/NPHP-2 localization was provided by mutants *hst-3.1(tm734)* and *rib-1(ok556)*, a gene that encodes an exostosin glycosyltransferase needed for HS elongation (Fig. 3 *B* and *C*; 44). These complete loss-of-function (i.e., null) alleles had defects in CFH-1 and inversin/NPHP-2 localization comparable to those found in *hst-3.1(em15)* (Fig. 3 *B* and *C*).

To confirm that the mutant phenotype was caused by a loss-of-function mutation in *hst-3.1*, and to identify whether the HST 3.1 protein was expressed in a cell-autonomous manner by CEP neurons or nonautonomously by another source tissue, we tested *hst-3.1* transgenes expressed under the control of tissue-specific promoters for rescue of the mutant phenotype. Although *hst-3.1* is expressed by body wall muscle and neurons (43), a *hst-3.1* transgene expressed under control of a muscle-specific promoter (*myo-3p::hst-3.1*) did not rescue the mutant phenotype. In contrast, *hst-3.1* transgenes expressed under control of a neuronal-specific *rgef-1* promoter and a dopaminergic neuron–specific *cat-2* promoter were able to rescue the mutant phenotype (Fig. 3 *B* and *C*), providing additional evidence that disruption of CFH-1 and inversin/NPHP-2 localization is the result of a loss-of-function mutation in *hst-3.1* and that the *hst-3.1* gene product likely modifies HS attached to a putative core proteoglycan synthesized by neurons. Like *hst-3.1(em15)*, loss-of-function mutations in this putative HS proteoglycan core protein would also be expected to disrupt CFH-1 and inversin/NPHP-2 localization.

Inversin/NPHP-2 and CFH-1 Localization Are Dependent on Syndecan/SDN-1. *C. elegans* has three HS-modified core proteoglycans associated with cell surfaces, the membrane-anchored glypicans,

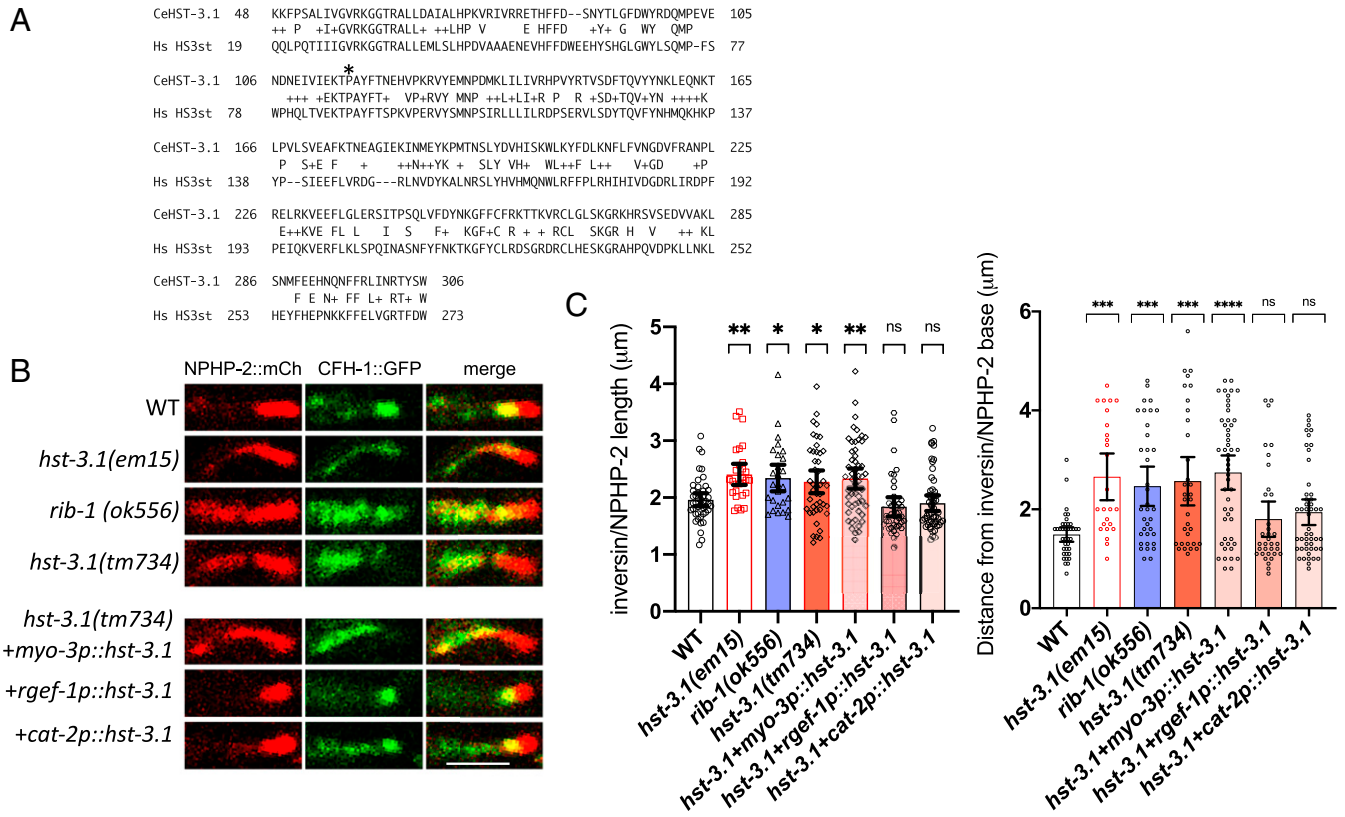

Fig. 3. HST-3.1 HS 3-*O* sulfotransferase prevents ectopic accumulation of inversin/NPHP-2 in distal cilia compartments. (*A*) BLAST alignment of *C. elegans* HST-3.1 and human HS 3 sulfotransferase protein sequences. The missense mutation in the *hst-3.1(em15)* mutant changes conserved Proline 116 (indicated by *) to a threonine. (*B*) A comparison of inversin/NPHP-2::mCherry and CFH-1::GFP localization in CEP neurons of WT, *hst-3.1(em15)*, *rib-1(ok556)*, and *hst-3.1(tm734)* mutant animals (*Top*) and *hst-3.1(tm734)* mutant animals expressing *hst-3.1* transgenes under the control of *myo-3*, *rgef-1*, and *cat-2* promoters (*Bottom*). All animals are day 3 adults. Note that inversin/NPHP-2::mCherry and CFH-1::GFP are restricted in WT animals but are diffuse in *hst-3.1* and *rib-1* mutants (*Top*). In contrast to the diffuse distributions of inversin/NPHP-2::mCherry and CFH-1::GFP in *hst-3.1(tm734)* mutant animals expressing a *hst-3.1* transgene under the control of a muscle-specific *myo-3 promoter*, the distributions of inversin/NPHP-2::mCherry and CFH-1::GFP are restricted in mutant animals expressing *hst-3.1* transgenes under the control of *rgef-1* and *cat-2* promoters (Scale bar, 2.5 μM). Anterior is oriented left in all images. (*C*) Scatter plots of inversin/NPHP-2 lengths in WT and *hst-3.1(em15)*, *rib-1 (ok556)*, and *hst-3.1(tm734)* mutant animals and *hst-3.1(tm734)* mutant animals expressing *hst-3.1* transgenes under the control of *myo-3*, *rgef-1*, and *cat-2* promoters (*Left*). Inversin/NPHP-2 lengths in *hst-3.1(em15)*, *rib-1(ok556)*, and *hst-3.1(tm734)* mutant animals and *hst-3.1(tm734)* mutant animals expressing *hst-3.1* transgenes under the control of *myo-3* promoters are statistically different from WT (as indicated by brackets with stars), while *hst-3.1* mutant animals expressing *hst-3.1* transgenes under the control of *rgef-1* and *cat-2* promoters are "rescued" and not statistically different from WT (ns). (*Right*) Scatter plots of CFH-1::GFP fluorescence peak locations in WT and *hst-3.1(em15)*, *rib-1(ok556)*, and *hst-3.1(tm734)* mutant animals and *hst-3.1(tm734)* mutant animals expressing *hst-3.1* transgenes under the control of *myo-3*, *rgef-1*, and *cat-2* promoters. *hst-3.1(em15)*, *rib-1(ok556)*, and *hst-3.1(tm734)* mutant animals and *hst-3.1(tm734)* mutant animals expressing *hst-3.1* transgenes under the control of *myo-3* promoters are statistically different from WT (as indicated by brackets with stars), while fluorescence peak location in *hst-3.1* mutant animals expressing *hst-3.1* transgenes under the control of *rgef-1* and *cat-2* promoters are "rescued" and are not statistically different from WT (ns). The error bars indicate 95% CIs. The significance is indicated by brackets with asterisks as follows: **P* < 0.1, ***P* < 0.01, ***P < 0.001, and *****P* < 0.0001; ns indicates no significant difference from WT.

GPN-1 and LON-2, and the transmembrane proteoglycan syndecan/SDN-1. To determine whether any of these HS-modified candidate proteoglycans are involved in CFH-1 and NPHP-2 distribution, CFH-1::GFP and NPHP-2::mCherry were placed in *gpn-1(ok377)*, *lon-2(e678)*, and *sdn-1(zh20)* mutant backgrounds. CFH-1::GFP and NPHP-2::mCherry distribution in glypican *gpn-1(ok377)* and *lon-2(e678)* mutant backgrounds were not significantly different from WT (Fig. 4 *A* and *B*). However, distribution of CFH-1::GFP and NPHP-2::mCherry was significantly disrupted in an *sdn-1(zh20)* mutant background, suggesting that syndecan/SDN-1 has a role in recruitment of CFH-1 on neuronal cell surfaces and in the mechanism that restricts inversin/NPHP-2 localization (Fig. 4).

To distinguish whether SDN-1 is expressed by CEP neurons and functions in a cell-autonomous manner, or whether SDN-1 is expressed from another source tissue and functions in a nonautonomous manner, we tested the inversin/NPHP-2 and CFH-1 phenotypes observed in an *sdn-1(zh20)* mutant background for rescue by *sdn-1* expressed under the control of the dopaminergic neuron–specific *cat-2* promoter. The *cat-2p::sdn-1* construct rescued inversin/NPHP-2 localization defects but unexpectedly did not rescue CFH-1 localization defects (Fig. 4 *A* and *B*). This discrepancy may be a dominant effect due to SDN-1 overexpression from the transgene since expression of the *cat-2p::sdn-1* transgene in a WT background also results in detectable CFH::GFP mislocalization (Fig. 4*B*).

To determine whether the cytoplasmic domain of SDN-1 is necessary to maintain inversin/NPHP-2 localization, a construct lacking the cytoplasmic domain of SDN-1 was tested for rescue of *sdn-1(zh20)* mutant phenotypes. The cytoplasmic deletion construct did not rescue inversin/NPHP-2 localization defects and resulted in increased defects in CFH-1 localization, consistent with the suggestion that that overexpression of the SDN-1 extracellular domain interferes with CFH-1::GFP localization (Fig. 4 *A* and *B*).

To determine SDN-1 localization on CEP neurons, a previously described SDN-1 construct with a cytoplasmic GFP tag (*opIs170*) (45) was crossed into a *sdn-1(zh20)* mutant background. However,

this construct was nonfunctional (i.e., it did not rescue the *sdn-1(zh20)* inversin/NPHP-2 localization defect) (Fig. 4*B*). Since fusion of GFP to the cytoplasmic domain of SDN-1 may interfere with its role in maintaining inversin/NPHP-2 distribution within its compartment, GFP was inserted into a *cat-2p*::*sdn-1* construct at the amino terminal of the extracellular domain, just after the signal sequence. This N-terminal *cat-2p*::GFP::SDN-1 fusion protein successfully rescued inversin/NPHP-2 localization defects and was therefore used to determine SDN-1 localization on CEP neurons (Fig. 4 *A* and *B*). Abundant GFP::SDN-1 was found throughout the CEP cell body and processes. Lower quantities of GFP::SDN-1 were also detected throughout CEP cilia, with localization most abundant in the regions flanking the proximal end of the inversin/NPHP-2 compartment and diffuse signal detected at the distal end of the inversin/NPHP-2 compartment that extended throughout the DS (Fig. 4*A*). GFP::SDN-1 localization on CEP neurons was similar in WT and *cfh-1(em14)* mutant backgrounds, indicating that although SDN-1 is necessary for correct CFH-1 distribution, the distribution of SDN-1 appears to be independent of CFH-1 (Fig. 4*A*).

sdn-1(zh20);hst-3.1(tm734) and *sdn-1(zh20);cfh-1(em14)* double mutants were tested for enhancement of mutant phenotypes to determine whether SDN-1, HST-3.1, and CFH-1 are likely to function in independent or overlapping pathways. The lack of enhancement of *sdn-1(zh20)* null mutant phenotypes by either *cfh-1(em14)* or *hst-3.1(tm734)* null mutants suggests that SDN-1, HST-3.1, and CFH-1 are likely to function in the same pathway or pathways with substantial overlap (Fig. 4 *B* and *C*). In support of this proposed mechanistic overlap with *cfh-1*, disruption of inversin/NPHP-2 localization in *sdn-1(zh20)* and *hst-3.1(tm734)* mutants was progressive and not observed in day 1 adults (*SI Appendix*, Fig. S5).

As an additional test to determine whether inversin/NPHP-2 defects arise as a consequence of CFH-1 mislocalization or represent CFH-1–independent functions of HST-3.1 and SDN-1, correlation analysis revealed moderate correlation between inversin/NPHP-2 length and CFH-1::GFP localization in a WT background ($r = 0.54$) that was slightly disrupted in *hst-3.1(tm734)* ($r = 0.38$) and more significantly disrupted in *sdn-1(zh20)* ($r = 0.10$; *SI Appendix*, Fig. S6). This supports the concept that HST-3.1 and SDN-1 mediate an interaction between CFH-1 and inversin/NPHP-2 that maintains inversin/NPHP-2 within its compartment.

CFH Restricts Inversin Localization in Mouse Photoreceptors. To determine whether the CFH-1–dependent localization of inversin/NPHP-2 described above is *C. elegans* specific or whether it is conserved in other species, we examined CFH and inversin/NPHP-2

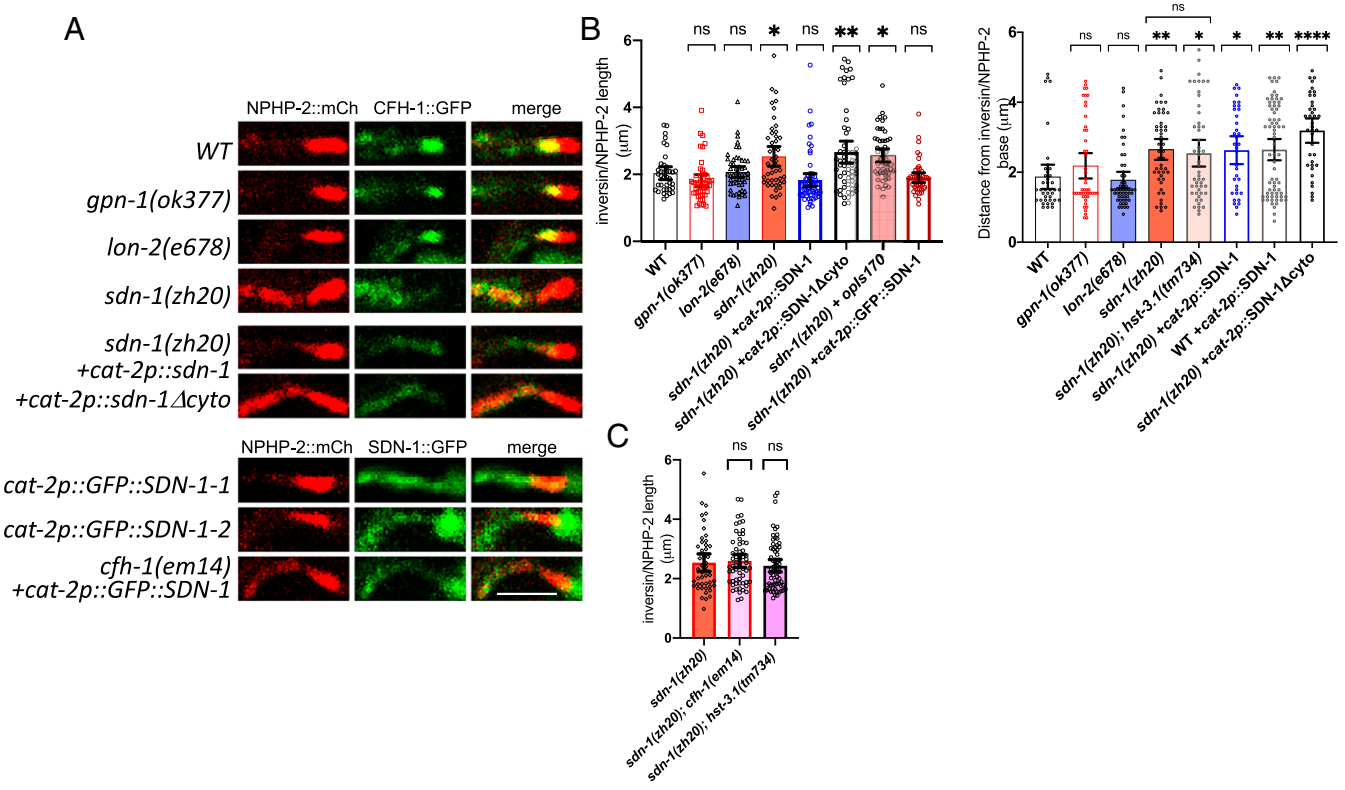

Fig. 4. Syndecan/SDN-1 prevents ectopic accumulation of inversin/NPHP-2 in distal cilia compartments. (*A*, *Top*) inversin/NPHP-2::mCherry and CFH-1::GFP distributions are restricted in WT, *gpn-1(ok377)*, and *lon-2(e678)* day 3 adults but are diffuse in *sdn-1(zh20)* day 3 adults. *sdn-1(zh20)* day 3 adults expressing a full-length *cat-2p::sdn-1* transgene have a restricted inversin/NPHP-2 distribution but diffuse CFH-1 distribution, while *sdn-1(zh20)* day 3 adults expressing a *cat-2p::sdn-1* transgene missing the *sdn-1* cytoplasmic domain have a diffuse distribution of both inversin/NPHP-2 and CFH-1. (*Bottom*) Inversin/NPHP-2 mCherry and GFP::SDN-1 distribution in two different WT day 3 adult animals and a *cfh-1(em14)* day 3 adult (Scale bar, 2.5 μM). Anterior is oriented left in all images. (*B*, *Left*) Scatter plots of inversin/NPHP-2 lengths in WT, *gpn-1(ok377)*, *lon-2(e678)*, *sdn-1(zh20)*, and *sdn-1(zh20)* animals containing *cat-2p::sdn-1* transgenes with intact and missing cytoplasmic domains (Δcyto) and *sdn-1* transgenes with C-terminal (*opIs170*) and N-terminal (GFP::SDN-1) GFP tags. (*Right*) scatter plots of CFH-1::GFP fluorescence peak locations in WT, *gpn-1(ok377)*, *lon-2(e678)*, *sdn-1(zh20)*, *sdn-1(zh20);hst-3.1(tm734)*, *sdn-1(zh20)*, and WT animals with transgenes containing *cat-2p::sdn-1* transgenes and *sdn-1(zh20)* animals with transgenes containing *cat-2p::sdn-1* transgenes with missing cytoplasmic domains (Δcyto). Also indicated is the comparison of CFH-1::GFP fluorescence peak locations between *sdn-1(zh20)* single and *sdn-1(zh20);hst-3.1(tm734)* double mutants that shows no significant difference (upper bracket). (*C*) Scatter plots showing no significant differences between inversin/NPHP-2 lengths in *sdn-1(zh20)* single mutant and *sdn-1(zh20);cfh-1(em14)* and *sdn-1(zh20);hst-3.1(tm734)* double mutants. The error bars indicate 95% CIs. The significance is indicated by brackets with asterisks as follows: *$P < 0.1$, **$P < 0.01$, ***$P < 0.001$, and ****$P < 0.0001$; ns indicates no significant difference from WT.

localization in mouse retina. To identify CFH localization in the retina, eye sections from WT and cfh$^{-/-}$ knockout mice (21- and 19-wk-old males, respectively) were stained with CFH antibodies. In agreement with previously published data, antibodies to CFH intensely stained photoreceptor inner segments in WT retina (46, 47), and this staining was absent in the retina of cfh$^{-/-}$ mice (Fig. 5*A*), indicating that the inner-segment antibody staining is dependent on the presence of CFH and not an immunofluorescence artifact.

To test whether CFH has a role in maintenance of inversin/NPHP-2 localization in mouse photoreceptors similar to that described above for CFH-1 in *C. elegans* sensory neurons, retina sections from WT and cfh$^{-/-}$ knockout mice with no sign of photoreceptor degeneration were stained with well-characterized antibodies to inversin/NPHP-2 (48, 49) and rhodopsin (used as a marker for photoreceptor outer segments). Inversin/NPHP-2 appears concentrated exclusively in photoreceptor inner segments in WT animals. In contrast, inversin/NPHP-2 is found ectopically in photoreceptor outer segments in cfh$^{-/-}$ mice (Fig. 5*B*). This finding suggests that CFH has an evolutionarily conserved role in preventing inversin/NPHP-2 accumulation in ectopic cellular compartments in multiple neuronal cell types in both invertebrate and vertebrate species and that the relationship between these two proteins is apparently conserved even outside the context of cilium structure.

Inversin Localization Is Defective in High-AMD–Risk Y402H Photoreceptors. Two regions of CFH, within CCP 7 and CCP 19 to 20, mediate interaction with cell surface HS (10). Sequence variants in these regions not only reduce interaction with HS but are also thought to result in an elevated risk for AMD (6). Humans homozygous for CFH Y402H, where tyrosine 402 in CCP 7 is replaced by a histidine, for example, have a sixfold increase in AMD risk compared to Y402 homozygotes, although the mechanism that links decreased HS binding to AMD pathogenesis remains unclear (1–4). Since the observations in *C. elegans* described above indicate that CFH-1 and HS modification regulate inversin/NPHP-2 localization, we wanted to determine whether amino acid Y402 in human CFH has a significant role in localization of inversin/NPHP-2. Comparison of postmortem retina sections from two Y402 and two Y402H individuals with no sign of disease [unrelated males between 52 and 68 y old (50)] revealed distinct patterns of inversin/NPHP-2 distribution. Inversin is concentrated in puncta in the outer segments of low-AMD–risk Y402 photoreceptors, with little or no staining detected in photoreceptor inner segments. In contrast, inversin has a diffuse distribution with abundant staining throughout photoreceptor inner and outer segments in the Y402H homozygous high-AMD–risk background (Fig. 5*C*). This suggests that, in addition to its roles in mediating CFH–HS interactions and AMD risk, Y402 inhibits ectopic localization of inversin/NPHP-2 in human photoreceptors. The reason for the distinct localization of inversin/NPHP-2 in the outer and inner segments of human and mouse photoreceptors, respectively, is not clear. However, distinct distributions for several other photoreceptor components have been identified that make it worth considering whether differences in molecular organization and physiological function might be responsible for the distinct photoreceptor phenotypes that result from the same genetic lesions in the two species and contribute to some of the challenges in establishing a widely accepted mouse AMD model (51–53).

Discussion

The experiments described here investigate the function of CFH-1, a *C. elegans* protein with structural similarity to vertebrate CFH, sharing N-terminal signal sequences followed by 20 tandem CCP modules. Although this structural homology is striking, the sequences within the 20 tandem CCP modules are divergent (*SI Appendix*, Fig. S1), making evolutionary orthology appear uncertain, despite an earlier analysis that makes this claim (29).

Observations of noncanonical functions for vertebrate CFH, in tandem with the absence of homologs of vertebrate CFH-interacting proteins CFI and C3 in *C. elegans*, suggests that CFH-1 may also have functions and interact with partners that are outside of the alternative complement pathway (17, 18, 54). In this respect, the expression of CFH-1 by a class of dopaminergic mechanosensory neurons in *C. elegans* (Fig. 1) is unexpected and intriguing since, to our knowledge, vertebrate CFH has no established neuronal functions. Interestingly, earlier work by others indicates that the eight tandem CCP modules found in the *C. elegans* LEV-9 protein are required for organization of postsynaptic acetylcholine receptors, demonstrating that some CCP protein modules have ancient, noncanonical functions in organizing sensory machinery at neuromuscular junctions that predate separation of the nematode and vertebrate lineages (55).

CFH-1–Mediated Regulation of Inversin/NPHP-2 Assembly. As far as we can tell, GFP::CFH-1 does not have a synaptic localization like LEV-9 (55); however, the localization of GFP::CFH-1 on mechanosensory neuron cilia (Fig. 1) suggests that CFH-1 may also function in the structural organization of a sensory apparatus. Ectopic assembly of inversin/NPHP-2 in two distinct *cfh-1* null mutants that is rescued by introduction of a WT *cfh-1* transgene (Fig. 2) supports this suggestion and indicates that CFH-1 may have a role in maintaining inversin compartment boundaries or in a poorly understood mechanism that regulates the length of inversin/NPHP-2 fibrillar structures (28). This CFH-1 function seems to be specific for inversin/NPHP-2 regulation since two ciliary proteins in adjacent locations, ARL-13 and TRP-4, seem surprisingly unaffected by loss of CFH-1. Moreover, the role of CFH-1 in modulating inversin/NPHP-2 assembly appears to be evolutionarily conserved, since loss of CFH function is also associated with ectopic accumulation of inversin/NPHP-2 in mouse and human photoreceptors (Fig. 5).

The association between inversin/NPHP-2 and CFH in mouse photoreceptors is particularly striking since both proteins are associated with the inner segment of the photoreceptors, providing evidence for an association between CFH and inversin/NPHP-2 that can occur even outside the cilium. Interestingly, accumulation of inversin/NPHP-2 in the distal ciliary compartment appears to be age dependent in *C. elegans*. Although ectopic inversin/NPHP-2 accumulation in mouse and human photoreceptors was not examined at different time points, the age-dependent increase in accumulation seen in *C. elegans* (Fig. 2) may have implications for the progressive dysfunction of photoreceptors in humans with AMD (see below).

Interaction of CFH-1 with HS. HS are linear repeats of glucuronic and *N*-acetylglucosamine disaccharides with heterogenous structures due to variations in disaccharide repeat length and in multiple modifications that include epimerization, acetylation, and sulfation by selective 2-, 3-, and 6-*O* HS sulfotransferases (13). Although 3-*O* modification contributes only an estimated 0.5% of sulfate in HS, evolutionary conservation of seven *hst-3* genes in vertebrates suggests that this modification has important developmental and/or homeostatic functions (13, 56). It is thought that 3-*O* modification regulates HS ligand specificity and has roles in neuronal synaptogenesis and branching in *C. elegans* (43, 57).

Although we have not established direct binding between CFH-1 and HS or SDN-1, the identification of mutations in *hst-3.1* that disrupt CFH-1 and inversin/NPHP-2 localization suggest that CFH-1 is a ligand whose functional interaction with HS is potentially regulated by HS 3-*O* modification, at least in *C. elegans*. Defective CFH-1 and inversin/NPHP-2 localization in a null mutant of *rib-1*, a gene that encodes an exostosin glycosyltransferase required for HS elongation, supports this role. Moreover, rescue of a *hst-3.1* mutant with a *hst-3.1* transgene

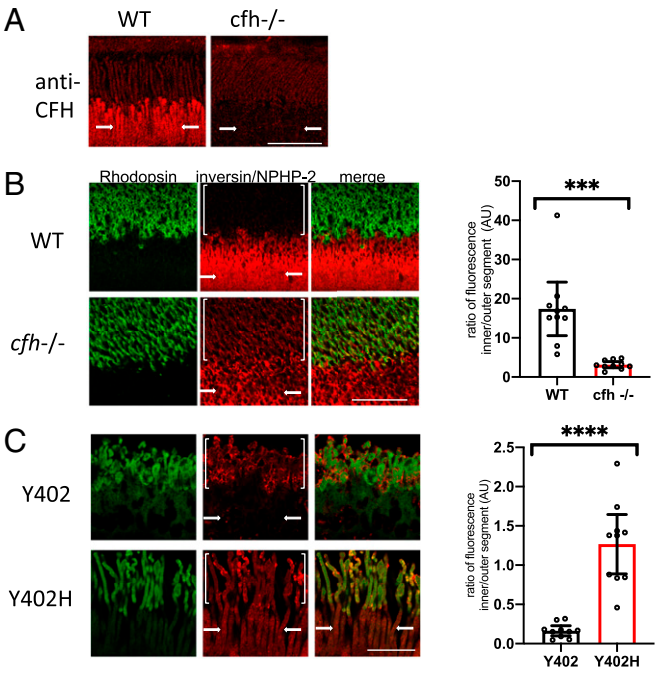

Fig. 5. CFH restricts inversin/NPHP-2 distribution in vertebrate photoreceptors. (*A*) Antibody staining of WT and CFH$^{-/-}$ mouse retina with Santa Cruz anti-CFH antibody (SC-17951) demonstrates that photoreceptor inner-segment staining (arrows) is dependent on the presence of intact CFH gene. (*B*) Antibody staining of mouse retina sections reveal that inversin/NPHP-2 is restricted to inner segment of WT mouse photoreceptors (*Top*, arrows) but is detected in both inner and outer segments (brackets) of photoreceptors in *cfh*$^{-/-}$ mice. (*Right*) Scatter plot of ratio of relative NPHP-2 fluorescence levels in inner segment divided by outer segment in WT and cfh$^{-/-}$ mutant animals. The error bars indicate 95% CIs. The significant difference from WT is indicated by brackets with asterisks as follows: ***$P < 0.001$. (*C*) Antibody staining of human retina sections reveals that inversin/NPHP-2 is concentrated in puncta in outer segments (brackets) of low-AMD–risk Y402 homozygotes (*Top*) with little or no detectable staining in photoreceptor inner segments (arrows). In contrast, inversin/NPHP-2 has a diffuse distribution in high-AMD–risk Y402H homozygotes with abundant staining detected in photoreceptor inner segments (arrows). (*Right*) Ratio of NPHP-2 fluorescence levels in IS divided by OS in Y402 and Y402H human retinas. The error bars indicate 95% CIs. The significant difference from WT is indicated by brackets with asterisks as follows: ****$P < 0.0001$ (Scale bar, 20 μm). Posterior is oriented up in all images.

expressed under the control of two neuron-specific promoters indicates that the HST-3.1 enzyme likely modifies HS attached to a proteoglycan core protein produced by neurons that acts as a receptor for CFH-1. Analysis of inversin/NPHP-2 and CFH-1 localization in a *sdn-1(zh20)* mutant background suggests (but does not prove) that syndecan/SDN-1 is the core proteoglycan modified by HST-3.1 that not only recruits CFH-1 but also mediates CFH-1–dependent localization of inversin/NPHP-2 (Fig. 4).

This is supported by the overlap and age dependence of *cfh-1*, *hst-3.1*, and *sdn-1* phenotypes by the demonstration that dopaminergic neuron–specific expression of a *cat-2p::sdn-1* transgene rescues the *sdn-1* mutant phenotype and that deletion of the syndecan/SDN-1 cytoplasmic domain disrupts ability of the transgene to rescue this phenotype (Fig. 4). Although direct binding has not been established, the lack of enhancement of *sdn-1(zh20)* phenotypes in double mutants with *cfh-1(em14)* and *hst-3.1(tm734)* supports the suggestion that these three proteins function in the same pathway or pathways with significant overlap. A schematic summarizing the localization of HS modified syndecan/SDN-1 core proteoglycan, CFH-1, and inversin/NPHP-2 is shown in Fig. 6.

Interestingly, a syndecan paralog and inversin/NPHP-2 are respectively required in zebrafish and mouse cilia to establish left-right axes during embryogenesis, suggesting that syndecans and inversin/NPHP-2 may also have functional overlap in vertebrate cilia that are related to those described here (26, 58).

Noncanonical Role for CFH Interaction with HS and Its Possible Implications for AMD. A CFH Y402H variant that is simultaneously thought to reduce HS binding (10) and result in a sixfold increase in AMD risk is shown to have ectopic inversin/NPHP-2 accumulation in human photoreceptors (Fig. 5). This data suggests that the role for CFH-1 and HS in modulation of inversin/NPHP-2 accumulation in *C. elegans* mechanosensory neurons may be evolutionarily conserved in human photoreceptors.

A substantial fraction of neurodegenerative retinal disease results from defects in cilia structure and trafficking (59), making the concept that cilia defects also contribute to the pathogenetic mechanism of photoreceptor degeneration seen in AMD seem worthy of consideration. The concept that a defect in inversin/NPHP-2 regulation contributes to defects in photoreceptor function and survival seems reasonable since a mutation in inversin/NPHP-2 is associated with Retinitis Pigmentosa in at least one patient with Senior–Loken syndrome (60). Although photoreceptor dysfunction in AMD is thought to be the consequence of a primary defect in retinal pigmented epithelial (RPE) cells caused by proinflammatory fatty deposits (i.e., drusen) at RPE basal surfaces (8, 17), the results presented here dovetail with studies showing that the symptoms of macular degeneration, including RPE and choroid defects, can result from primary structural and signaling defects in photoreceptors and their primary cilia (20, 21, 61). Although the accumulation of lipid-rich drusen at RPE basal surfaces is the first clinical sign of disease, it is conceivable that there are molecular changes in RPE and/or photoreceptor function that occur prior to the histologic changes used for AMD diagnosis. It may be noteworthy that defects in RMDA have been detected in AMD patients with the CFH Y402H variant prior to the appearance of other clinical AMD symptoms such as drusen accumulation (19).

In further support of this concept, a recent study indicates that in addition to AMD, individuals with the CFH Y402H variant also have an elevated risk for the neurodegenerative retinal ciliopathy, Retinitis Pigmentosa (62). Based on the canonical function of CFH, the authors suggest that defective regulation of the alternative complement pathway may contribute to the pathogenesis of Retinitis Pigmentosa (62). However, data presented here suggest another possible interpretation: The Y402H variant of CFH results in a photoreceptor cilia defect that increases risk for both AMD and Retinitis Pigmentosa.

Materials and Methods

***C. elegans* Strains.** A list of the *C. elegans* strains used in this work is included in *SI Appendix*, Table S1.

CRISPR-Cas9. CRISPR-Cas9 technology was used to delete 7 nt of genomic sequence from the F36H2.3 gene (F36H2 25890-25896) to create a frameshift in *cfh-1* coding sequence and nonsense codon and Xba-1 restriction site. CRISPR-Cas9 technology was also used to insert GFP in frame into *cfh-1* coding sequence at the same location as described (32). The sequence of the crisper RNA (crRNA) was AACAGCACAATACCGTATCT (Dharmacon). The repair template used to create the deletion had a 35 nt overlap with endogenous sequence on both sides of the Cas9 cleavage site and had the sequence, GCGTGGTTTTGACAACTCAACAGCACAATACCGTATCTAGATTTATCAGTACGAGGATATGAAAGAACAGAAAGTG (Integrated DNA Technologies). The forward and reverse primers used to amplify GFP also had 35 nt overlaps with endogenous sequence on either side of the Cas9 cleavage site,

GTGGTTTTGACAACTCAACAGCACAATACCGTATCCGAGCTCGAATTCAAGTACC

and CTTTCATATCCTCGTACTGATAAATCTTCATCCGACCAGGACATGTAAGCTTGTG.

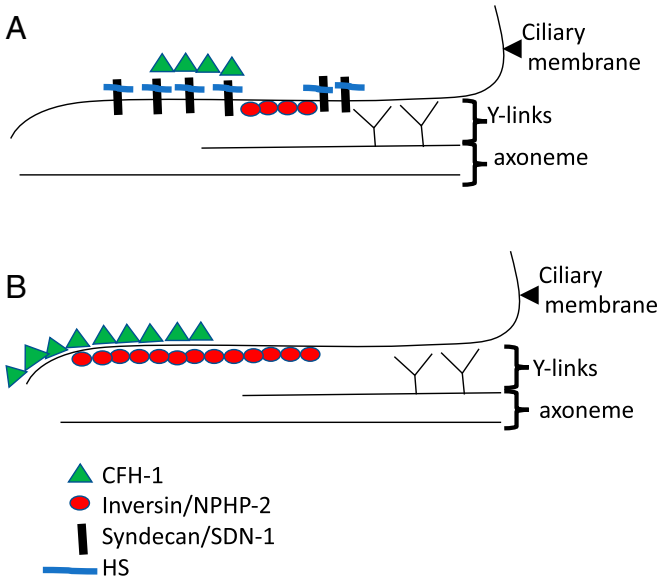

Fig. 6. A schematic diagram summarizing relative locations of inversin/NPHP-2, CFH-1, and HS-modified syndecan/sdn-1 on sensory neuron cilia. (*A*) In WT animals, CFH-1 (green triangle) is in a fairly restricted region located to the distal end of the inversin/NPHP-2 compartment (red ovals). HS (blue line) attached to syndecan proteoglycan (black line) has a diffuse distribution in regions flanking the proximal and distal ends of the inversin/NPHP-2 compartment. (*B*) In the absence of SDN-1, HS, or HS modification by HS 3-O sulfotransferase, CFH-1 has a diffuse distribution on the cilia membrane, and inversin/NPHP-2 accumulation is no longer restricted to a small region of the MS but extends into the DS. Note that the schematic diagrams depict half of a cilium with ciliary membrane, axoneme, and Y-links in each image.

Cas9 nuclease was a generous gift from Dominique Rasoloson and Geraldine Seydoux. Injection mixtures were prepared as described, including *dpy-10* crRNA and repair template as coinjection markers, and injected into the gonad of N2 hermaphrodites (32, 63). *dpy-10* progeny were screened by PCR for insertion of *cfh-1* repair templates.

Generation of ARL-13::mNeonGreen Using CRISPR/Cas9. Worm-optimized mNeonGreen (mNG) (64) was knocked in to the endogenous *arl-13* locus to generate *arl-13(oq118)*/ARL-13::mNG using a *dpy-10* co-CRISPR strategy (32). Custom synthesized crRNA specific to the 3′ end of *arl-13* (GTGAAAAAAGGAGGTTATTT) was ordered from IDT. High-fidelity PCR was used to generate a linear mNG repair template with 35 bp homology arms using the following primers: TTCAAAACGTTCTGAACAATCGAGTAGTGCCAAAAGGAACCGGAGGTGGCGGATCTGG and aagtgtttatggcttcaaaagtgaaaaaaggaggTCACTTGTAGAGTTCATCCATTC. Sanger sequencing confirmed the accuracy of the knock-in allele.

Analysis of Calcium Responses with GCaMP6s. Transgenic WT and *cfh-1* mutant adults containing a plasmid expressing GCaMP-6s under the control of the *dat-1* promoter were placed on an agar plate with small patches of food and allowed to freely crawl between lawn patches. The plate was placed on an inverted microscope and imaged with a 5× objective, on a custom-built microscope (BioVision). Images were acquired with an Orca Flash 4.0 complementary metal oxide semiconductor camera (Hamamatsu) at 5 Hz with a 50 ms exposure to decrease motion artifacts and manually tracked with a motorized stage (Applied Sciences). Samples were illuminated with a Sola light-emitting diode (Lumnecor) and enhanced GFP filter set (ET49002, Chroma). Neurons were tracked and quantified using custom software (MATLAB).

Basal Slowing Assay. Basal slowing assays were performed as described (40). Animals of various ages were washed in M9 buffer and placed in the center of a 2 cm ring of HB101 bacteria. A "blinded" experimenter who did not know the genotype of the different worm strains counted the number of body bends in a 20 s interval before and 20 s interval after the worms entered the bacteria. The experiment was repeated three times with $n = 10$ animals per experiment.

Mutant Screening and Identification. Young adult animals containing an integrated NPHP-2::mCherry transgene expressed under the control of *dat-1* 5′ regulatory sequence in tandem with a CRISPR-Cas9–mediated insertion of GFP into *cfh-1* coding sequence (described above) were mutagenized with ethyl methanesulfonate. F2 animals were anesthetized with phenoxypropanol and placed on a 5% agar pad on a microscope slide. Animals were screened for abnormal NPHP-2::mCherry localization on an Olympus BX51 microscope, and individual mutant animals were recovered from the slide, cloned to an individual plate, and allowed to recover. The progeny of cloned mutant animals were checked for NPHP-2::mCherry and CFH-1::GFP mislocalization on a Nikon A1R confocal microscope with Nikon Elements Software.

The *hst-3.1* mutation was identified by a combination of whole-genome sequencing and mapping via MIP-MAP (42). Briefly, the mutation-bearing strain was crossed to strain VC20019, and mutant (homozygous) F2 progeny were transferred to a new plate with food. Upon starvation, the worms were washed from the plate and used for genomic DNA isolation. Mapping libraries were constructed with MIP designed to detect VC20019-derived single-nucleotide polymorphisms (SNPs). In parallel, standard next-generation sequencing (NGS) libraries were constructed using TruSeq DNA sample prep kit version 2 or TruSeq ChIP sample prep kit (Illumina) for whole-genome sequencing. The MIP and NGS libraries were pooled and subjected to single-end 50 bp sequencing (HiSEq. 2500; Illumina), producing >1,000 and >25× coverage, respectively. SNP frequencies from the MIP library were plotted against the physical map, revealing a mapping interval between 2 and 8 Mbp on chromosome II. Six candidate mutations (homozygous, nonsynonymous coding variants) from the NGS library were identified as described (65) using a pipeline of BBMAP (https://sourceforge.net/projects/bbmap/), SAMtools (66), FreeBayes (67), and ANNOVAR (68). Mutations in candidate genes were examined for phenotypic overlap with the isolated *em15* mutant, and on this basis, *hst-3.1* was selected for further study.

Immunofluorescence and Microscopy. Adult *C. elegans* were immobilized for 10 min with 15 μM levamisole (LKT Laboratories) in M9 buffer and placed on a 5% agar pad on a microscope slide. Imaging was performed with a Nikon A1R confocal microscope with Nikon Elements software.

Postmortem human and mouse eyes were embedded in paraffin and sectioned as described (47, 50). Sectioned eyes were deparaffinized in Xylene and hydrated through 100, 95, 70, and 50% ethanol washes (3 min each). After washing in PBS, sections were postfixed in 4% paraformaldehyde in PBS and blocked in 5% goat or donkey serum in PBS containing 0.3% Triton-X-100. Sections were stained with mouse monoclonal antibody 4D2 to rhodopsin (Novus Biologicals), rabbit polyclonal antibody to inversin (Proteintech 10585-1-AP), or Santa Cruz anti-CFH antibody (SC-17951) and secondary goat or donkey anti-mouse and anti-rabbit IgG with fluorescent tags. After mounting in KPL fluorescent mounting medium, slides were imaged using a Nikon A1R confocal microscope with Nikon Elements Software.

Transmission electron microscopy of the CEP cilium was conducted on chemically fixed day 1 adult worms as previously outlined (69).

Statistical Analysis. One-way ANOVA followed by Tukey's or Dunnett's multiple comparisons test and correlation analysis were performed using GraphPad Prism version 8.0.0 for Windows (GraphPad Software, https://www.graphpad.com/).

Data Availability. All study data are included in the article and/or *SI Appendix*.

ACKNOWLEDGMENTS. We thank Maria Doitsidou, Hannes Bulow, Inna Nechipurenko, Piali Sengupta, Maureen Barr, Victor Jensen, Michel Leroux, and Mervyn Monteiro for their exceptional generosity in sharing *C. elegans* strains and constructs and Dominique Rasoloson, Alexander Paix, Geraldine Seydoux, Amy Fabritius, and Tyler Hansen for CRISPR-Cas9 reagents and assistance. In addition, we thank Roxana Radu for providing tissue from *cfh* $^{-/-}$ mice obtained originally from Matthew Pickering and Gregory Hageman. We also thank Andy Ziman for assistance with microscopy, Murray Pressman, Shengyun Fang, and Jon Lederer for helpful discussions, and Zubair Ahmed and Saumil Sethna for comments on the manuscript. B.E.V. is supported by funding from NIH Grant R21EY030188. J.A.M. is supported by the Canadian Institutes of Health Research. H.S. and A. Golden are supported by the Intramural Research Program of the NIH, National Institute of Diabetes and Digestive and Kidney Diseases. Some *C. elegans* strains were provided by the CGC, which is funded by NIH Office of Research Infrastructure Programs (P40 OD010440), and the *C. elegans* Reverse Genetics Core Facility at the University of British Columbia, which is part of the international *C. elegans* Gene Knockout Consortium.

1. A. O. Edwards *et al*., Complement factor H polymorphism and age-related macular degeneration. *Science* **308**, 421–424 (2005).
2. G. S. Hageman *et al*., A common haplotype in the complement regulatory gene factor H (HF1/CFH) predisposes individuals to age-related macular degeneration. *Proc. Natl. Acad. Sci. U.S.A.* **102**, 7227–7232 (2005).
3. J. L. Haines *et al*., Complement factor H variant increases the risk of age-related macular degeneration. *Science* **308**, 419–421 (2005).
4. R. J. Klein *et al*., Complement factor H polymorphism in age-related macular degeneration. *Science* **308**, 385–389 (2005).
5. S. Zareparsi *et al*., Strong association of the Y402H variant in complement factor H at 1q32 with susceptibility to age-related macular degeneration. *Am. J. Hum. Genet.* **77**, 149–153 (2005).
6. S. Raychaudhuri *et al*., A rare penetrant mutation in CFH confers high risk of age-related macular degeneration. *Nat. Genet.* **43**, 1232–1236 (2011).
7. L. G. Fritsche *et al*., Age-related macular degeneration: Genetics and biology coming together. *Annu. Rev. Genomics Hum. Genet.* **15**, 151–171 (2014).
8. C. B. Toomey, L. V. Johnson, C. Bowes Rickman, Complement factor H in AMD: Bridging genetic associations and pathobiology. *Prog. Retin. Eye Res.* **62**, 38–57 (2018).
9. M. J. Walport, Complement. First of two parts. *N. Engl. J. Med.* **344**, 1058–1066 (2001).
10. S. J. Clark *et al*., Tissue-specific host recognition by complement factor H is mediated by differential activities of its glycosaminoglycan-binding regions. *J. Immunol.* **190**, 2049–2057 (2013).
11. M. Bernfield *et al*., Functions of cell surface heparan sulfate proteoglycans. *Annu. Rev. Biochem.* **68**, 729–777 (1999).
12. H. E. Bülow, O. Hobert, The molecular diversity of glycosaminoglycans shapes animal development. *Annu. Rev. Cell Dev. Biol.* **22**, 375–407 (2006).
13. U. Lindahl, J. P. Li, Interactions between heparan sulfate and proteins-design and functional implications. *Int. Rev. Cell Mol. Biol.* **276**, 105–159 (2009).
14. F. E. Poulain, H. J. Yost, Heparan sulfate proteoglycans: A sugar code for vertebrate development? *Development* **142**, 3456–3467 (2015).
15. J. Turnbull, A. Powell, S. Guimond, Heparan sulfate: Decoding a dynamic multifunctional cell regulator. *Trends Cell Biol.* **11**, 75–82 (2001).
16. A. Langford-Smith, T. D. Keenan, S. J. Clark, P. N. Bishop, A. J. Day, The role of complement in age-related macular degeneration: Heparan sulphate, a ZIP code for complement factor H? *J. Innate Immun.* **6**, 407–416 (2014).
17. C. B. Toomey, U. Kelly, D. R. Saban, C. Bowes Rickman, Regulation of age-related macular degeneration-like pathology by complement factor H. *Proc. Natl. Acad. Sci. U.S.A.* **112**, E3040–E3049 (2015).
18. B. Calippe *et al*., Complement factor H inhibits CD47-mediated resolution of inflammation. *Immunity* **46**, 261–272 (2017).
19. R. F. Mullins *et al*., The ARMS2 A69S polymorphism is associated with delayed rod-mediated dark adaptation in eyes at risk for incident age-related macular degeneration. *Ophthalmology* **126**, 591–600 (2019).
20. R. Ayyagari *et al*., X-linked recessive atrophic macular degeneration from RPGR mutation. *Genomics* **80**, 166–171 (2002).
21. S. M. Conley *et al*., Insights into the mechanisms of macular degeneration associated with the R172W mutation in RDS. *Hum. Mol. Genet.* **23**, 3102–3114 (2014).
22. J. F. Reiter, M. R. Leroux, Genes and molecular pathways underpinning ciliopathies. *Nat. Rev. Mol. Cell Biol.* **18**, 533–547 (2017).
23. E. A. Otto *et al*., Mutations in INVS encoding inversin cause nephronophthisis type 2, linking renal cystic disease to the function of primary cilia and left-right axis determination. *Nat. Genet.* **34**, 413–420 (2003).
24. D. Shiba *et al*., Localization of Inv in a distinctive intraciliary compartment requires the C-terminal ninein-homolog-containing region. *J. Cell Sci.* **122**, 44–54 (2009).
25. S. R. Warburton-Pitt *et al*., Ciliogenesis in Caenorhabditis elegans requires genetic interactions between ciliary middle segment localized NPHP-2 (inversin) and transition zone-associated proteins. *J. Cell Sci.* **125**, 2592–2603 (2012).
26. D. Morgan *et al*., Inversin, a novel gene in the vertebrate left-right axis pathway, is partially deleted in the inv mouse. *Nat. Genet.* **20**, 149–156 (1998).
27. L. Sang *et al*., Mapping the NPHP-JBTS-MKS protein network reveals ciliopathy disease genes and pathways. *Cell* **145**, 513–528 (2011).
28. H. W. Bennett *et al*., Novel fibrillar structure in the inversin compartment of primary cilia revealed by 3D single-molecule superresolution microscopy. *Mol. Biol. Cell* **31**, 619–639 (2020).
29. J. Krushkal, C. Kemper, I. Gigli, Ancient origin of human complement factor H. *J. Mol. Evol.* **47**, 625–630 (1998).
30. W. Kim, R. S. Underwood, I. Greenwald, D. D. Shaye, OrthoList 2: A new comparative genomic analysis of human and *Caenorhabditis elegans* genes. *Genetics* **210**, 445–461 (2018).
31. R. Hunt-Newbury *et al*., High-throughput in vivo analysis of gene expression in Caenorhabditis elegans. *PLoS Biol.* **5**, e237 (2007).
32. A. Paix, A. Folkmann, D. Rasoloson, G. Seydoux, High efficiency, homology-directed genome editing in Caenorhabditis elegans using CRISPR-Cas9 ribonucleoprotein complexes. *Genetics* **201**, 47–54 (2015).
33. N. J. Bialas *et al*., Functional interactions between the ciliopathy-associated Meckel syndrome 1 (MKS1) protein and two novel MKS1-related (MKSR) proteins. *J. Cell Sci.* **122**, 611–624 (2009).
34. L. D. Jayanthi *et al*., The Caenorhabditis elegans gene T23G5.5 encodes an antidepressant- and cocaine-sensitive dopamine transporter. *Mol. Pharmacol.* **54**, 601–609 (1998).
35. M. Wojtyniak, A. G. Brear, D. M. O'Halloran, P. Sengupta, Cell- and subunit-specific mechanisms of CNG channel ciliary trafficking and localization in C. elegans. *J. Cell Sci.* **126**, 4381–4395 (2013).
36. S. R. Warburton-Pitt, M. Silva, K. C. Nguyen, D. H. Hall, M. M. Barr, The nphp-2 and arl-13 genetic modules interact to regulate ciliogenesis and ciliary microtubule patterning in C. elegans. *PLoS Genet.* **10**, e1004866 (2014).
37. W. Li, Z. Feng, P. W. Sternberg, X. Z. A C. Xu, A C. elegans stretch receptor neuron revealed by a mechanosensitive TRP channel homologue. *Nature* **440**, 684–687 (2006).
38. S. Cevik *et al*., Active transport and diffusion barriers restrict Joubert Syndrome-associated ARL13B/ARL-13 to an Inv-like ciliary membrane subdomain. *PLoS Genet.* **9**, e1003977 (2013).
39. C. elegans Deletion Mutant Consortium, Large-scale screening for targeted knockouts in the Caenorhabditis elegans genome. *G3 (Bethesda)* **2**, 1415–1425 (2012).
40. E. R. Sawin, R. Ranganathan, H. R. Horvitz, C. elegans locomotory rate is modulated by the environment through a dopaminergic pathway and by experience through a serotonergic pathway. *Neuron* **26**, 619–631 (2000).
41. Y. Tanimoto *et al*., In actio optophysiological analyses reveal functional diversification of dopaminergic neurons in the nematode C. elegans. *Sci. Rep.* **6**, 26297 (2016).
42. C. A. Mok *et al*., MIP-MAP: High-Throughput mapping of *Caenorhabditis elegans* temperature-sensitive mutants via molecular inversion probes. *Genetics* **207**, 447–463 (2017).
43. E. Tecle, C. A. Diaz-Balzac, H. E. Bülow, Distinct 3-*O*-sulfated heparan sulfate modification patterns are required for kal-1-dependent neurite branching in a context-dependent manner in Caenorhabditis elegans. *G3 (Bethesda)* **3**, 541–552 (2013).
44. H. Kitagawa *et al*., Expression of rib-1, a Caenorhabditis elegans homolog of the human tumor suppressor EXT genes, is indispensable for heparan sulfate synthesis and embryonic morphogenesis. *J. Biol. Chem.* **282**, 8533–8544 (2007).
45. C. Rhiner, S. Gysi, E. Fröhli, M. O. Hengartner, A. Hajnal, Syndecan regulates cell migration and axon guidance in C. elegans. *Development* **132**, 4621–4633 (2005).
46. M. N. Mandal, R. Ayyagari, Complement factor H: Spatial and temporal expression and localization in the eye. *Invest. Ophthalmol. Vis. Sci.* **47**, 4091–4097 (2006).
47. Z. Smit-McBride *et al*., Localization of complement factor H gene expression and protein distribution in the mouse outer retina. *Mol. Vis.* **21**, 110–123 (2015).
48. F. Suizu *et al*., Phosphorylation-dependent Akt-Inversin interaction at the basal body of primary cilia. *EMBO J.* **35**, 1346–1363 (2016).
49. Y. Nakajima, H. Kiyonari, Y. Mukumoto, T. Yokoyama, The Inv compartment of renal cilia is an intraciliary signal-activating center to phosphorylate ANKS6. *Kidney Int.* **93**, 1108–1117 (2018).
50. J. C. Wang *et al*., CFH Y402H polymorphism is associated with elevated vitreal GM-CSF and choroidal macrophages in the postmortem human eye. *Mol. Vis.* **21**, 264–272 (2015).
51. A. el-Amraoui *et al*., Human usher 1B/mouse shaker-1: The retinal phenotype discrepancy explained by the presence/absence of myosin VIIA in the photoreceptor cells. *Hum. Mol. Genet.* **5**, 1171–1178 (1996).
52. T. A. Mavlyutov, H. Zhao, P. A. Ferreira, Species-specific subcellular localization of RPGR and RPGRIP isoforms: Implications for the phenotypic variability of congenital retinopathies among species. *Hum. Mol. Genet.* **11**, 1899–1907 (2002).
53. C. Brennenstuhl *et al*., Targeted ablation of the Pde6h gene in mice reveals cross-species differences in cone and rod phototransduction protein isoform inventory. *J. Biol. Chem.* **290**, 10242–10255 (2015).
54. M. Nonaka, Evolution of the complement system. *Subcell. Biochem.* **80**, 31–43 (2014).
55. M. Gendrel, G. Rapti, J. E. Richmond, J. L. Bessereau, A secreted complement-control-related protein ensures acetylcholine receptor clustering. *Nature* **461**, 992–996 (2009).
56. N. W. Shworak *et al*., Pathway-specific regulation of the synthesis of anticoagulantly active heparan sulfate. *J. Biol. Chem.* **269**, 24941–24952 (1994).
57. M. I. Lázaro-Peña, C. A. Díaz-Balzac, H. E. Bülow, S. W. Emmons, Synaptogenesis is modulated by heparan sulfate in *Caenorhabditis elegans*. *Genetics* **209**, 195–208 (2018).
58. C. B. Arrington, A. G. Peterson, H. J. Yost, Sdc2 and Tbx16 regulate Fgf2-dependent epithelial cell morphogenesis in the ciliated organ of asymmetry. *Development* **140**, 4102–4109 (2013).
59. K. L. Bales, A. K. Gross, Aberrant protein trafficking in retinal degenerations: The initial phase of retinal remodeling. *Exp. Eye Res.* **150**, 71–80 (2016).
60. J. F. O'Toole, E. A. Otto, Y. Frishberg, F. Hildebrandt, Retinitis pigmentosa and renal failure in a patient with mutations in INVS. *Nephrol. Dial. Transplant.* **21**, 1989–1991 (2006).
61. S. Y. Cheng *et al*., Altered photoreceptor metabolism in mouse causes late stage age-related macular degeneration-like pathologies. *Proc. Natl. Acad. Sci. U.S.A.* **117**, 13094–13104 (2020).
62. A. Sodi *et al*., CFH Y402H polymorphism in Italian patients with age-related macular degeneration, retinitis pigmentosa, and Stargardt disease. *Ophthalmic Genet.* **39**, 699–705 (2018).
63. J. A. Arribere *et al*., Efficient marker-free recovery of custom genetic modifications with CRISPR/Cas9 in Caenorhabditis elegans. *Genetics* **198**, 837–846 (2014).
64. N. C. Shaner *et al*., A bright monomeric green fluorescent protein derived from *Branchiostoma lanceolatum*. *Nat. Methods* **10**, 407–409 (2013).
65. H. E. Smith, S. Yun, Evaluating alignment and variant-calling software for mutation identification in C. elegans by whole-genome sequencing. *PLoS One* **12**, e0174446 (2017).
66. H. Li *et al*.; 1000 Genome Project Data Processing Subgroup, The sequence alignment/map format and SAMtools. *Bioinformatics* **25**, 2078–2079 (2009).
67. E. Garrison, G. Marth, Haplotype-based variant detection from short-read sequencing. arXiv [Preprint] https://arxiv.org/abs/1207.3907 (20 July 2012).
68. K. Wang, M. Li, H. Hakonarson, ANNOVAR: Functional annotation of genetic variants from high-throughput sequencing data. *Nucleic Acids Res.* **38**, e164 (2010).
69. A. A. Sanders, J. Kennedy, O. E. Blacque, Image analysis of Caenorhabditis elegans ciliary transition zone structure, ultrastructure, molecular composition, and function. *Methods Cell Biol.* **127**, 323–347 (2015).